Proc. Schl. Eng. Tokai Univ., Ser. E
39 (2014) 73-80

Skid Control of Small Electric Vehicles (Direct Yaw Moment Control using Tire Steer Angle)

by

Mohamad Heerwan Bin PEEIE[*1], Hirohiko OGINO[*2] and Yasuo OSHINOYA[*2]

(Received on Mar. 31, 2014 and accepted on July 14, 2014)

Abstract

Due to the space limitation of the driving tire, some small electric vehicles with two in-wheel motors employ a hydraulic-mechanical brake system (HMBS) as a braking system. Although the mechanical braking system is compact, the rigidness and the response performance of the mechanical braking system is lower than a hydraulic braking system. On the other hand, a small electric vehicle only employs a seat belt as safety equipment, and there is no antilock braking system (ABS), which is a basic skid control system. Furthermore, the inertia moment of the rear tire is larger than the front one because an in-wheel motor was attached to the rear tire. During braking and disturbance, due to the disadvantage of the mechanical braking system and the large inertia moment of the rear tire, the vehicle easily loses its stability, increasing the possibility of an accident. In this paper, to increase the stability and the safety of the small electric vehicle with two in-wheel motors, we propose a novel method based on the yaw moment of the vehicle. This method is known as a direct yaw moment control (DYC) using tire steer angle. The state feedback control method and the feedback gain matrix for tire steer angle have been used in our model. The input of this system is the tire steering angle while the output is the yaw angular velocity and the side slip angle of the vehicle. The simulation result shows that during braking and disturbance, DYC can improve the vehicle motion for the driver desired direction and increase the stability of the vehicle.

Keywords: Direct Yaw Moment Control (DYC), Skid Control, In-wheel Motor, Hydraulic-Mechanical Brake System (HMBS), Small Electric Vehicle

1. Introduction

In recent years, due to the growing needs on energy and environment protection, electrified driving system is gradually gaining attention in the automobile industry [1]. Compared with internal combustion engine vehicles (ICVs), in-wheel motor have great advantages such as, quick torque response, motor torque can be measured easily and motor can be attached at each wheel. These advantages of in-wheel motor enhance vehicle motion control in the small electric vehicle [2].

For a small electric vehicle with in-wheel motor at the rear tire (also known as driving tire), due to space limitation, an anti-lock braking system (ABS) that is a basic skid control system is difficult to install. For the same reason, mechanical braking system is installed at the driving tire. Although the mechanical braking system is compact, our past research has proved that the rigidness and response performance of the mechanical braking system is lower than hydraulic braking system [3-5]. When a vehicle brakes on an icy road or during emergency braking, the optimum braking pressure and the driver desired braking deceleration-g is difficult to obtain [6, 7]. As a result, the vehicle will be skidding on an icy road and the possibility of an accident will be increased. Based on the disadvantages of the mechanical braking system, we can say that a small electric vehicle that uses a hydraulic-mechanical brake system (HMBS) is not safe enough.

To increase the safety of the small electric vehicle, our past research has successfully constructed a simulation model of HMBS with ABS and regenerative brake control. The simulation result shows that ABS and regenerative brake control can prevent the vehicle from skidding during braking on an icy road [3-7]. On the other hand, we also have constructed a simulation model of HMBS with PID control to obtain the driver desired braking deceleration-g. The simulation result shows that PID control can obtain the driver desired braking deceleration-g [7, 8].

Although ABS and PID control can improve the safety

*1 Graduate Student, Course of Science and Engineering
*2 Professor, Department of Prime Mover Engineering

of the small electric vehicle, the stability of the vehicle is still need to be improved. To improve the stability of the vehicle, most previous studies have focused on yaw angular speed and side slip angle control [9-12]. However, to measure the side slip angle of the vehicle, we need the specific sensor such as a lateral acceleration sensor and the cost of that sensor is too expensive. On the other hand, many researchers were focused on the yaw moment control instead of the side slip angle [13-17]. Gyro sensor is the best sensor to measure the yaw angular velocity of the vehicle and the cost is cheap.

The aim of this study is to improve the stability of the small electric vehicle during braking on cornering. In this paper, we proposed the direct yaw moment control (DYC) using the front tire steer angle to increase the stability of the small electric vehicle with HMBS. In DYC system, the vehicle linear model has been used as an observer to obtain the optimum value of the yaw angular velocity and side slip angle of the small electric vehicle. The state feedback control method has been used in our observer to control the input of the state feedback system. From the algebraic Riccati equation, we can obtain the optimum value of the feedback gain and this feedback gain will be used as an input in the real model. This is the first step of our study on stability of the small electric vehicle and this paper only focused on to examine the effect of the optimal control to the vehicle stability. The effect of our proposed model has been validated in MATLAB/Simulink and the numerical analysis shows that our proposed model can give some positive impact to increase the stability of the vehicle.

2. Analysis Vehicle Model

2.1 Main symbols

B: braking force (N), I: inertia moment of the vehicle (kgm^2), L: length (m), P: pressure (Pa), R: regenerative brake, T: torque (Nm), W: wheel load (N), X: the longitudinal force acting on the tire (N), Y: the lateral force acting on the tire (N), C_R : regenerative brake coefficient, K_f and K_r : cornering stiffness for front and rear tire (N/rad), K_x and K_y: the rigidness of the tire in longitudinal axis and lateral axis (N/m^3), Y_d is the disturbance force (N), b and l: width and length of interacted tire surface (m), g: acceleration of gravity (m/s^2), f: friction force (N), h: center of gravity (m), l_f and l_r: the length from the center of the vehicle to the center of the front and rear tire (m), m: vehicle mass (kg), r: radius of the tire (m), t: time (s), u: vehicle velocity in the longitudinal direction (m/s), v: vehicle velocity in the lateral direction (m/s), β : side slip angle (rad), δ : steering angle (rad), γ : yaw angular velocity (rad/s), μ : friction coefficient, ρ : slip ratio, ω: tire angular velocity (rad/s)

Subscripts:

f : front, r : rear, fr : front right, fl : front left, rr : rear right, rl : rear left

2.2 Specifications of the analysis vehicle model

A small electric vehicle Toyota COMS (AK 10E-PC) has been used as an analysis vehicle model. Fig. 1 illustrates the small electric vehicle Toyota COMS (AK 10E-PC) while the specifications of this vehicle are provided in Table 1. This vehicle has several main features such as the direct in–wheel motors are attached at both rear tires and it has a hydraulic braking system at front tire and mechanical braking system at the rear tire. The combination of the front and rear braking system is called hydraulic-mechanical brake system (HMBS).

Table 1 Specifications of Toyota COMS

Vehicle mass	361.9 (kg)
Maximum speed	50 (km/h)
Height of center of gravity (CoG)	0.105 (m)
Tread front	0.840 (m)
Tread rear	0.815 (m)
Wheel base	1.280 (m)
Inertia of front tire	0.430 (kgm^2)
Inertia of rear tire	2.530 (kgm^2)
Driving system	2 in-wheel motors
Motor power output	0.290 (kW)
Lead acid batteries	6 sets, 12 (V), 33 (Ah)

2.3 Braking system of the analysis vehicle model

Fig. 2 shows the two-wheel model of the hydraulic-mechanical brake system (HMBS). In this model, the hydraulic braking system was installed at the front tire, while the mechanical brake system was installed at the rear tire, which is an in-wheel motor is located on the tire. When the driver pushes the braking pedal, the braking pressure generated from the master cylinder flows thru the front brake hose to the front wheel cylinder. On the other hand, for a mechanical brake system, the braking pressure generated

Figure. 1 Small electric vehicle Toyota COMS

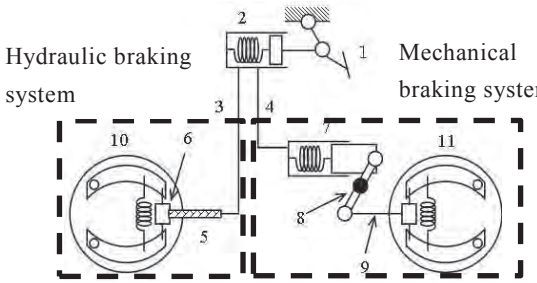

1:Brake Pedal 2:Master Cylinder 3:Front Brake Tube
4:Rear Brake Tube 5:Brake Hose 6:Wheel Cylinder
7:Power Cylinder 8:Link 9:Wire
10:Front Drum Brake 11:Rear Drum Brake

Figure 2 Hydraulic-mechanical brake system

in the master cylinder flow to the power cylinder, then the piston pulls a wire connected to the brake shoe. The equation of motion in power cylinder and drum brake is expressed in Eq. (1) and Eq. (2):

$$\rho g A_p H_p - k(x_p - x_d) - k_p x_p - d_p \frac{dx_p}{dt} = m_p \frac{d^2 x_p}{dt^2} \quad (1)$$

$$k(x_p - x_d) - k_d x_d - d_d \frac{dx_d}{dt} = m_d \frac{d^2 x_d}{dt^2} \quad (2)$$

where, A_p is an area of power cylinder, H_p is head pressure, k is the coefficient of the spring, d_p and d_d are viscous damping at power cylinder and drum brake, m_p and m_d are the mass of power cylinder and drum brake, x_p and x_d are displacement of spring at power cylinder and at drum brake and ρ is density of the brake fluid.

3. Numerical Calculation

3.1 Basic equations of motion

Fig. 3 shows the force vector at each wheel for the construction of basic equations of motion. The equations of motion in longitudinal and lateral direction are described as below [11]:

$$m\left(\frac{du}{dt} - vY\right) = \left(-X_{fr} - X_{fl}\right)\cos\theta + \left(-Y_{fr} - Y_{fl}\right)\sin\theta - X_{rr} - X_{rl} \quad (3)$$

$$m\left(\frac{dv}{dt} + uY\right) = \left(Y_{fr} + Y_{fl}\right)\cos\theta + \left(-X_{fr} - X_{fl}\right)\sin\theta + Y_{rr} + Y_{rl} + Y_d \quad (4)$$

From Eq. (4), Y_d is the disturbance and it is caused by the side wind. During braking, Y_d can affect the stability of the vehicle.

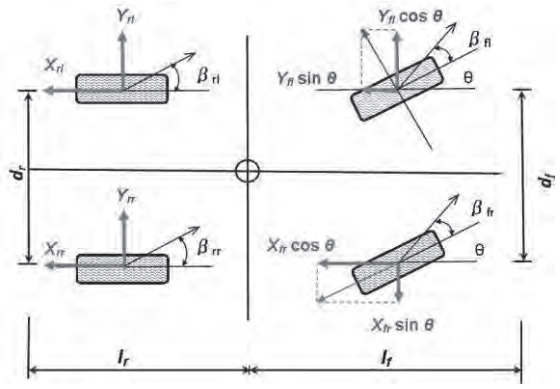

Figure 3 Force diagram of a vehicle

3.2 Direct yaw moment control (DYC)

The two wheels of the linear vehicle model has been used to construct an observer for DYC. The linear equations of motion to measure side slip angle, β and yaw angular velocity, γ of the vehicle are as below [12]:

$$mv\dot{\beta} + 2(K_f + K_r)\beta + \left[mv + \frac{2}{v}(l_f K_f - l_r K_r)\right] r = 2K_f \delta \quad (5)$$

$$2(l_f K_f - l_r K_r)\beta + I\dot{\gamma} + \frac{2(l_f^2 K_f + l_r^2 K_r)}{v} r = 2l_f K_f \delta \quad (6)$$

The cornering stiffness for the front and rear tire, K_f and K_r in Eq. (5) and Eq. (6) are the lateral force of the front and rear tire, Y_f and Y_r per unit side-slip angle of the front and rear tire, β_f and β_r. The equations of K_f and K_r are:

$$K_f = \frac{\partial Y_f}{\partial \beta_f} \quad (7)$$

$$K_r = \frac{\partial Y_r}{\partial \beta_r} \quad (8)$$

In our past research, we have used brush tire model to measure the lateral force and side slip angle of the tire [7-8]. The brush tire model allows elastic deformation in both the longitudinal and lateral directions [21]. From our past result, the relation of lateral force and side slip angle of the tire was shown in Fig. 4 and Fig.5. The value of K_f and K_r can be known from the gradient of an approximate line between the lateral force and side slip angle [22]. From Fig.4 and Fig.5, the value of K_f and K_r are -9756.1 N/rad and -7142.8 N/rad .

To describe a system in a linear motion, Eq. (5) and Eq.

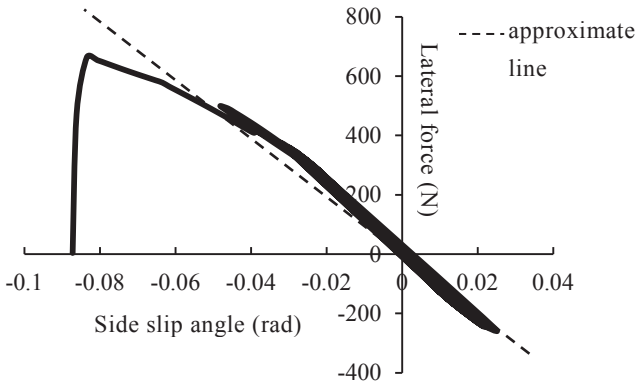

Figure 4 Lateral force and side slip angle of the front tire

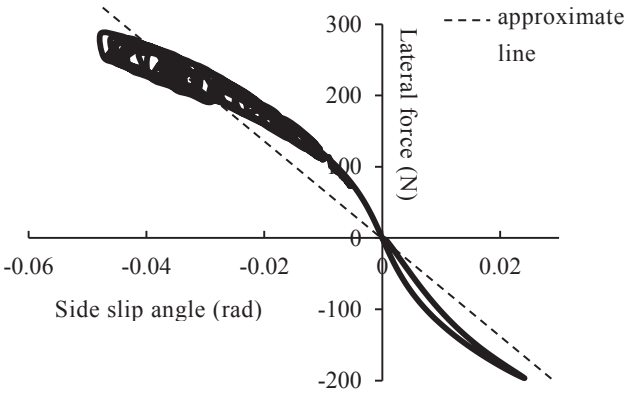

Figure 5 Lateral force and side slip angle of the rear tire

(6) can be transformed to the following equivalent linear state-space equation:

$$\dot{x} = Ax + bu \tag{9}$$

$$\begin{cases} y_1 = {c_1}^T x = \beta \\ y_2 = {c_2}^T x = \gamma \end{cases} \tag{10}$$

$${c_1}^T = [1 \quad 0]^T \ , \ {c_2}^T = [0 \quad 1]^T \tag{11}$$

where,

$$A = \begin{bmatrix} -\frac{2(K_f+K_r)}{mv} & -1-\frac{2(l_fK_f-l_rK_r)}{mv^2} \\ \frac{2}{I}(l_fK_f-l_rK_r) & -\frac{2({l_f}^2K_f+{l_r}^2K_r)}{Iv} \end{bmatrix} \tag{12}$$

$$x = [\beta \quad \gamma]^T \tag{13}$$

$$b = \begin{bmatrix} \frac{2K_f}{mv} \\ \frac{2l_fK_f}{I} \end{bmatrix} \tag{14}$$

$$u = \delta \tag{15}$$

Here, Eq. (12) and Eq. (14) can be simplified as:

$$A = \begin{bmatrix} a & b \\ c & d \end{bmatrix} \tag{16}$$

$$b = \begin{bmatrix} e \\ f \end{bmatrix} \tag{17}$$

where,

$$a = -\frac{2(K_f+K_r)}{mv} \quad , \quad b = -1-\frac{2(l_fK_f-l_rK_r)}{mv^2}$$

$$c = -\frac{2}{I}(l_fK_f - l_rK_r) \quad , \quad d = -\frac{2({l_f}^2K_f+{l_r}^2K_r)}{Iv}$$

$$e = \frac{2K_f}{mv} \quad , \quad f = \frac{2l_fK_f}{I}$$

In the state-space equation, x is a system state, u is a scalar representing the input of the system and y is a scalar representing the output of the system. The matrixes A, b and c determine the relationships between state and input and output variables. The block diagram of this system is shown in Fig. 6. In this system, the steering angle, δ is controlled by the driver.

To increase the stability of the vehicle, by using the state feedback control method, we used steering angle of the front tire and the feedback gain as an input in the observer. The feedback gain, g is proportional to the state vector, x. Then, the input system in a state-space equation is:

$$u = -g^T x + \delta_d \tag{18}$$

where,

$$g = [g_1 \quad g_2]^T \tag{19}$$

Substituting Eq. (18) into Eq. (9), gives:

$$\dot{x} = Ax + b(-g^T x + \delta_d)$$

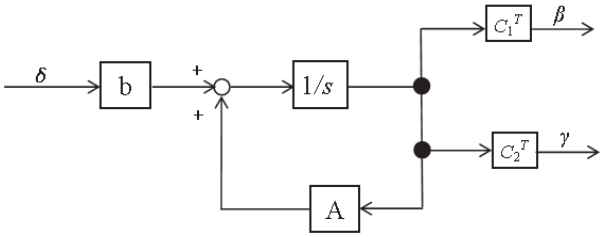

Figure 6 Block diagram of the vehicle with steering angle of the tire

$$\dot{x} = (\mathrm{A} - \mathrm{b}g^T)x + \delta_d \tag{20}$$

where δ_d is a steering angle of the front tire. The block diagram of the state-space form in Eq. (20) is shown in Fig. 7. In the observer, Linear Quadratic Regulator (LQR) problem is used to find the optimal state feedback. The evaluation function, *J* for Eq. (20) is:

$$\begin{cases} J = \int_0^\infty \left(x^T \mathrm{Q} x + R{\delta_d}^2\right) dt \\ \mathrm{Q} = \begin{bmatrix} q_{11} & 0 \\ 0 & q_{22} \end{bmatrix} \end{cases}$$

$$J = \int_0^\infty \left(q_{11}\beta^2 + q_{22}\gamma^2 + R{\delta_d}^2\right) dt \tag{21}$$

where q_{11} , q_{22} and *R* denote the state and input weighing matrixes. From Eq. (18), the optimal solution for the feedback gain is [13]:

$$u(t) = -\mathrm{g}(t)x \tag{22}$$

where

$$\mathrm{g} = R^{-1}\mathrm{b}^T\mathrm{P} \tag{23}$$

and $\mathrm{P} = \mathrm{P}^T \geq 0$ is the unique positive-semidefinite solution of the algebraic Riccati equation:

$$\mathrm{A}^T\mathrm{P} + \mathrm{PA} - \mathrm{Pb}R^{-1}\mathrm{b}^T\mathrm{P} = -\mathrm{Q}$$

$$\begin{bmatrix} a & b \\ c & d \end{bmatrix}^T \mathrm{P} + \mathrm{P}\begin{bmatrix} a & b \\ c & d \end{bmatrix} - \mathrm{P}\begin{bmatrix} e \\ f \end{bmatrix} R^{-1}[e \;\; f]\mathrm{P} = -\begin{bmatrix} q_{11} & 0 \\ 0 & q_{22} \end{bmatrix} \tag{24}$$

Here, P is defined as below:

$$\mathrm{P} = \begin{bmatrix} \varepsilon & \emptyset \\ \varphi & \gamma \end{bmatrix} \tag{25}$$

Then, substituting Eq. (25) into Eq. (24) gives:

$$\begin{bmatrix} a & c \\ b & d \end{bmatrix}\begin{bmatrix} \varepsilon & \emptyset \\ \varphi & \gamma \end{bmatrix} + \begin{bmatrix} \varepsilon & \emptyset \\ \varphi & \gamma \end{bmatrix}\begin{bmatrix} a & b \\ c & d \end{bmatrix} w^{-1}\begin{bmatrix} \varepsilon & \emptyset \\ \varphi & \gamma \end{bmatrix}\begin{bmatrix} e \\ f \end{bmatrix}[e \;\; f]\begin{bmatrix} \varepsilon & \emptyset \\ \varphi & \gamma \end{bmatrix} = -\begin{bmatrix} q_{11} & 0 \\ 0 & q_{22} \end{bmatrix}$$

$$\therefore \begin{cases} (a\varepsilon + c\varphi) + (a\varepsilon + c\emptyset) - \frac{1}{w}[e\varepsilon(e\varepsilon + f\emptyset) + f\varphi(e\varepsilon + f\emptyset)] = q_{11} \\ (a\emptyset + c\gamma) + (b\varepsilon + d\gamma) - \frac{1}{w}e\emptyset(e\varepsilon + f\emptyset) + f\gamma(e\varepsilon + f\emptyset) = 0 \\ (b\varepsilon + d\varphi) + (a\varphi + c\gamma) - \frac{1}{w}[e\varepsilon(e\varphi + f\gamma) + f\varphi(e\varphi + f\gamma)] = 0 \\ (b\emptyset + d\gamma) + (b\varphi + d\gamma) - \frac{1}{w}[e\emptyset(e\varphi + f\gamma) + f\gamma(e\varphi + f\gamma)] = q_{22} \end{cases} \tag{26}$$

where q_{11}, q_{22} and R were set as constant weighing matrixes by the designer. The relation between q_{11}, q_{22} and R are

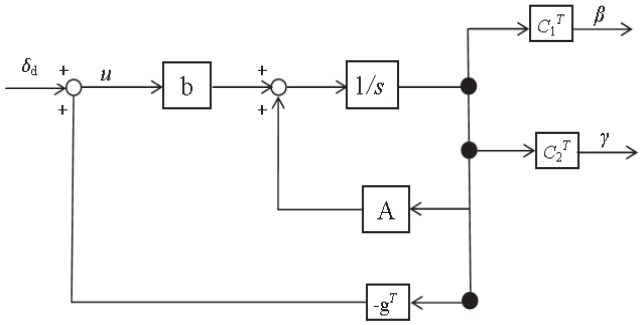

Figure 7 Block diagram of the state feedback control with the gain feedback and steering angle as an input

Table 2 Relation of weighing matrixes to the state output and input of the system

Large	Fix	|x|	|ẋ|	|u|
q_{11}	q_{22}, R	Decrease	Increase	Increase
q_{22}	q_{11}, R	Increase	Decrease	Increase
R	q_{11},q_{22}	Increase	Increase	Decrease

q_{22}. In the numerical analysis, the value of q_{11}, q_{22} and R were set as 1, 1 and 3.

shown in Table 2. Based on the Table 2, to increase the value of state, x, the weighing input, R must be more than q_{11} and

4. Result and Discussions

In the numerical calculation, the initial velocity of the vehicle is 30 km/h, the initial steering angle is 5 degrees and the road is dry asphalt. The braking system of the vehicle is hydraulic-mechanical brake system without ABS and the initial braking pressure is 1.8 MPa. This baking pressure is constant until the vehicle is completely stopped. The disturbance force is 1 kN and this force will start hitting the vehicle from 1 second to 2 second. In the numerical calculation, we have set two cases as:

1. Case 1: The vehicle was cornering with disturbance and DYC was non-operational.
2. Case 2 : The vehicle was cornering with disturbance and DYC was operational.

4.1 Effect of the DYC using tire steer angle to the motion of the vehicle

In this part, before we examine the effect of our DYC to the vehicle motion, we have examined the effect of the disturbance to the vehicle and tire rotational speed. This result is necessary for us because ABS was not applied in our braking system and the possibility of the tire lock occurs

during braking and disturbance is high. Fig. 8 shows the changes of the vehicle and tire rotational speed during cornering and the disturbance was occuring form 1 *sec* to 2 *sec*. From Fig. 8, it is shows that the disturbance was not effect the vehcile speed and tire rotational speed although ABS was not applied in the braking system. This result approved that during braking on the dry asphalt, due to the large friction coefficent of the road, the hydraulic-mechanical braking system can obtain the optimum braking force to the all tires.

Then, we have examined the effect of the DYC to the trajectories of the vehicle. Fig. 9 shows the trajectories of the vehicle for all cases. From Fig. 9, the trajectories of the vehicle in case of DYC operational is more steer compared with the case of DYC non-operational. During cornering and disturbance, due to the large load at rear tire and weight movement at each tire, the motion of the vehicle will be in an under steer condition. However, in case of DYC using tire steer angle was operational, the vehicle can improve its steer performance. This result is approved that our proposed model can improve the motion of the vehicle during cornering and disturbance.

4.2 Effect of the DYC using tire steer angle to the vehicle stability

In order to investigate the effect of our proposed model to the stability of the vehicle, we have examined the result of the yaw moment velocity of the vehicle,γ and side slip angle of the vehicle,β. Fig. 10 shows the changes of γ during cornering and disturbance. From Fig. 10, the value of γ in case of the DYC non-operational is increased from 0 rad/s to 0.24 rad/s in 1.5 sec, then from 1.5 sec to 5 sec, the value of γ was decreased gradually from 0.24 rad/s to 0 rad/s. In case of DYC operational, the value of γ was increased from 0 rad/s to 0.20 rad/s in 1 sec, then from 1 sec to 4 sec, the value of γ

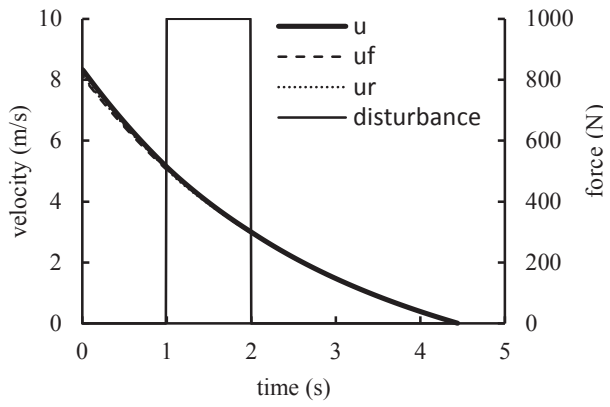

Figure 8 Changes of the vehicle and tire rotational speed during cornering and disturbance

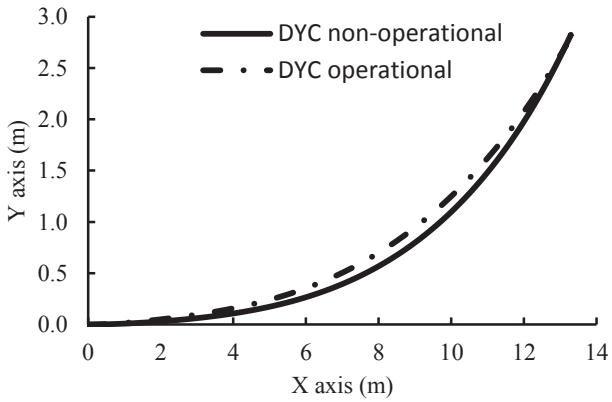

Figure 9 Trajectories of the vehicle in case of DYC operational and non-operational

was decreased gradually from 0.2 rad/s to 0 rad/s. During the disturbance, from 1 sec to 2 sec, the value of γ was not increased. However, in case of DYC non-operational, during the disturbance, the value of γ was increased. From this result, it can be said that by using our proposed model, we can obtain the optimum value of the γ although the disturbance was occurring.

Fig. 11 shows the changes of the β in case of DYC operational and non-operational during cornering and disturbance. From this result, in case of DYC non-operational, the value of β was increased from 0 rad to 0.018 rad in 0.3 sec, then from 0.3 sec to 1 sec, the value of β was decreased to 0.012 rad. When the disturbance was occurring, from 1 sec to the vehicle completely stopped, the value of β was increased gradually from 0.12 rad to 0.04 rad. In case of DYC operational, from 0 sec to 0.02 sec, the value of β was increased rapidly to 0.025 rad. Then from 0.02 sec to 1 sec, the value of β was decreased rapidly from 0.025 *rad* to 0.005 rad. However, when the disturbance was occurring, from 1 sec to 3 sec, the value of β was increased gradually to 0.03 rad, and after 3 sec to the end, the value of β was decreased approach to 0 *rad*. From this result, it shows that during

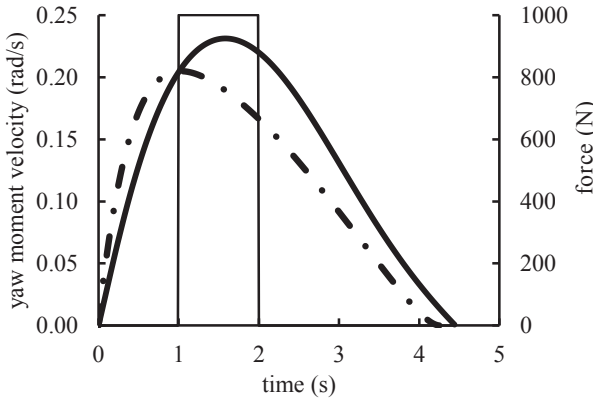

Figure 10 Changes of the yaw moment velocity of the vehicle in case of DYC operational and non-operational

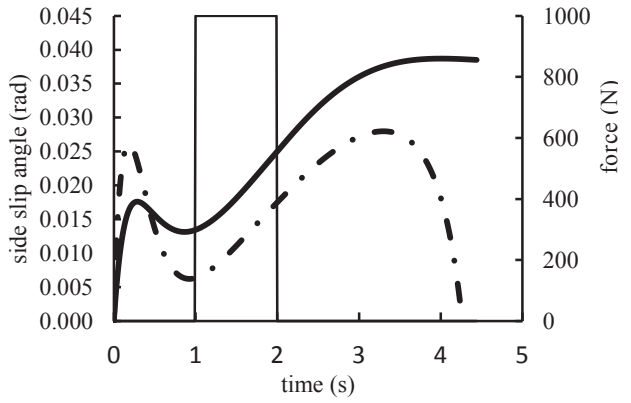

Figure 11 Changes of the side slip angle of the vehicle in case of DYC operational and DYC non0operational

cornering and disturbance, by using our proposed model, we can improved the value of β.

5. Conclusions

In this study, to improve the stability of the small elelctric vehicle with two in-wheel motors, we have constructed the novel method of the DYC using tire steer angle. The simulation has been done in the conditions of the vehicle was braking on the cornering and the disturbance was hitting the vehicle from 1 sec to 2 sec. From the simulation results, we found that several conditions must be needed in our simulation to increase the stability of the vehicle:

1. The velocity of the vehicle must be constant.
2. The changes of the lateral velocity must be small.

References

1) Z.Zhang, L.Xiong and Z.Yu: The Anti-Skidding Control for Hybrid-Braking System, Proceeding of the 2010 IEEE International Conference on Vehicular Electronics and Safety, pp. 36-41, (2010).
2) K.Fujii and H.Fujimoto: Traction Control Based on Slip Ratio Estimation without Detecting Vehicle Speed for Electric Vehicle, Proceedings of the 2007 Power Conversion Conference, pp. 688-693, (2007).
3) S.Hasegawa and H.Ogino: Research on Skid Control of Small Electric Vehicle with Hydraulic-Mechanical Hybird Brake System -1st Report: Simulation of 2 Wheel Model of Anti-Lock Braking System-, Proceedings of the School of Engineering, Tokai University, Vol.49, No.2, pp. 89-94, (2009), (in Japanese).
4) S.Kobayashi and H.Ogino: Research on Skid Control of Small Electric Vehicle with Hydraulic-Mechanical Hybird Brake System -Simulation of 4 Wheel Brake Model-, Proceedings of the 2010 JSME Conference, Vol.5, pp. 165-166, (2010), (in Japanese).
5) H.Ogino, S.Hasegawa and S.Kobaayshi: Research on Skid Control of Small Electric Vehicle with Hydraulic-Mechanical Hybird Brake System -2nd Report: Effect of the Mechanical Braking Force-, Proceedings of the School of Engineering, Tokai University, Vol.50, No.1, pp. 69-77 (2010), (in Japanese).
6) M.I.Ishak, H.Koduki and H.Ogino: Research on Anti-Lock Braking System of a 2 Wheel Small Electric Vehicle with Hydraulic-Mechanical Hybrid Brake System, Proceedings of the 2010 JSAE Kanto International Conference of Automotive Technology for Young Engineers (ICATYE) (2010), CD-ROM.
7) M.Heerwan, H.Ogino, Y.Oshinoya: Skid Control of Small Electric Vehicle -Effect of the PI Controller to the Brake Performance-, Proceedings of the 2012 JSME Transportation and Logistics Conference (2012), CD-ROM.
8) M.Heerwan, H.Ogino, Y.Oshinoya: Skid Control of Small Electric Vehicle -Effect of the PID Controller to the Brake Performance-, Proceedings of the JSAE Annual Congress (Spring) (2013), CD-ROM.
9) T.Chung and K.Yi: Design and Evaluation of Side Slip Angle-Based Vehicle Stability Control Scheme on a Virtual Test Track, IEEE Transactions on Control System Technology, Vol.14, No.2, pp. 224-234, (2006).
10) L.Wei, L.Wenying, D.Haito and G.Konghui: Side-slip Angle Estimation for Vehicle Electronic Stability Control Based on Sliding Mode Observer, Proceedings of the 2012 International Conference on Measurement, Information and Control, pp. 992-995, (2012).
11) W.Yihu, S.Dandan, H.Zhixiang and Y.Xiang: A Fuzzy Control Method to Improve Vehicle Yaw Stability Based on Integrated Yaw Moment Control and Active Front Steering, Proceedings of the 2007 IEEE International Conference on Mechatronics and Automation, pp. 1508-1512, (2007).
12) W.Wang, L.Yuan, S.Tao,W.Zhang and T.Su: Estimation of Vehicle Side Slip Angle in Nonlinear Condition Based on the State Feedback Observer, Proceedings of the 2010 IEEE International Conference on Automation and Logistics, pp. 632-636, (2010).
13) DY.Kim, C.Kim, S.Kim and J.Choi: Development of Adaptive Direct Yaw Moment Control Method for Electric Vehicle Based on Identification of Yaw Rate Model, Proceeding of the Intelligent Symposium (IV), pp. 1098-1103, (2011).
14) Y.Aoki, Z.Li and Y.Hori: Robust Design of Body Slip Angle Observer with Cornering Power Identification at Each Tire for Vehicle Motion Stabilization, Proceeding of the 9th IEEE International Workshop on Advanced Motion Control (AMC), pp. 590-595, (2006).

15) W.Liang, H.Yu, R.McGee, M.Kuang and J.Medanic: Vehicle Pure Yaw Moment Control using Differential Tire Slip, Proceedings of the 2009 American Control Conference, pp. 3331-3336, (2009).
16) H.Fujimoto, A.Tsumasaka and T.Noguchi: Direct Yaw-moment Control of Electric Vehicle Based on Cornering Stiffness Estimation, Proceedings of the Industrial Electronics Society, pp. 2626-2631, (2005).
17) L.R Ray: Nonlinear State and Tire Force Estimation for Advanced Vehicle Control, IEEE Transaction on Control System Technology, Vol. 3, No. 1, pp. 117-124, (1995).
18) M.Abe: Vehicle Handling Dynamics, pp. 30-37, (2009).
19) M.Abe: Vehicle Handling Dynamics, pp. 54, (2009).
20) Sigud Skogested and Ian Postlethwaite: Multivariable Feedback Control Analysis and Design, pp. 376, (2005).
21) M.Abe: Vehicle Handling Dynamics, pp. 30, (2009).
22) T.Hiraoka, O.Nishihara and H.Kumamoto: Path Tracking of Four Wheel Steering Vehicle by Using Sliding Mode Control, Transaction of The Institute of System, Control and Information Engineers, Vol. 16, No. 10, pp. 520-530, (2003)